

Complexity-Aware Deep Symbolic Regression with Robust Risk-Seeking Policy Gradients

Zachary Bastiani^{1,2} Robert M. Kirby^{1,2} Jacob Hochhalter³ Shandian Zhe¹

¹ Kahlert School of Computing ² Scientific Computing and Imaging Institute

³ Department of Mechanical Engineering

University of Utah

{u0450013, jacob.hochhalter}@utah.edu

{kirby, zhe}@cs.utah.edu

Abstract

We propose a novel deep symbolic regression approach to enhance the robustness and interpretability of data-driven mathematical expression discovery. Our work is aligned with the popular DSR framework which focuses on learning a data-specific expression generator, without relying on pretrained models or additional search or planning procedures. Despite the success of existing DSR methods, they are built on recurrent neural networks, solely guided by data fitness, and potentially meet tail barriers that can zero out the policy gradient, causing inefficient model updates. To overcome these limitations, we design a decoder-only architecture that performs attention in the frequency domain and introduce a dual-indexed position encoding to conduct layer-wise generation. Second, we propose a Bayesian information criterion (BIC)-based reward function that can automatically adjust the trade-off between expression complexity and data fitness, without the need for explicit manual tuning. Third, we develop a ranking-based weighted policy update method that eliminates the tail barriers and enhances training effectiveness. Extensive benchmarks and systematic experiments demonstrate the advantages of our approach.

1 Introduction

Symbolic regression (SR) (Schmidt and Lipson, 2009; Jobin et al., 2019; Rudin, 2019) is an important research direction for achieving interpretability in machine learning. Given a dataset that records the input and output of a complex system of interest, symbolic regression seeks to discover a simple, concise equation that reveals the system’s underlying mechanism — thereby enhancing our understanding and ensuring the model’s reliability.

Genetic programming (GP) (Koza, 1994; Randall et al., 2022; Burlacu et al., 2020) has long been the dominant approach for symbolic regression. However, GP is known to be computationally expensive and time-consuming due to its evolutionary nature. (Bomarito et al., 2023) introduces a variant GP that leverages fractional Bayes factor to indicate the most likely expression for noisy datasets. Deep Symbolic Regression (DSR) (Petersen et al., 2019) and its variants (Tenachi et al., 2023; Jiang et al., 2024) represent a recent breakthrough by training a recurrent neural network (RNN) to generate expressions from data efficiently. While DSR has demonstrated success across many SR benchmarks, the RNN-based architecture can struggle with capturing long-range dependencies and is prone to vanishing gradients (Hochreiter, 1998), especially in large expression trees. In addition, DSR methods typically rely on data-fitting rewards, which can lead to overly complex expressions and overfitting — particularly in noisy settings. Furthermore, due to the usage of the reward difference as the weights in the policy gradients, DSR takes the risk of meeting tail barriers, *i.e.*, zero policy gradients, which can result in inefficient model updates.

Another emerging line of research leverages large pretrained foundation models that map datasets directly to expression (or token) generators (Kamienny et al., 2022; Valipour et al., 2021). These generators are then integrated into a complex, iterative search process to optimize the resulting expressions (Shojaee et al., 2023; Holt et al., 2023; Kamienny et al., 2023). While promising, these methods are highly dependent on the quality of the pretrained models, which are costly to obtain and sensitive to the choice of training data. Moreover, effectively coordinating the pretrained model with the downstream search or planning steps is non-trivial yet crucial for success.

Our work aligns with the DSR framework, which we view as a promising direction due to its independence from costly pretraining and additional search and planning mechanism. Our approach focuses on learning a data-specific expression generator. To improve the interpretability, accuracy, and runtime of the DSR paradigm, we introduce a robust, complexity-aware deep symbolic regression method (CADSR). Our major contributions are summarized as follows:

- **Expression Model.** We design a decoder-only architecture that performs attention in the frequency space. Specifically, we apply the discrete cosine transform to the embeddings to obtain their frequency representations. High-frequency components — often attributed to noise, outliers, or excessive parameter perturbations — are removed, and attention is computed over the resulting low-frequency components. An inverse transform is then applied to recover updated embeddings in the original space. Next, to enhance the model’s ability to capture positional information within the expression tree, we introduce a dual-indexed positional encoding based on both the depth and horizontal location of each token. We use a breadth-first search (BFS) strategy to generate the expression tree layer by layer, which offers both computational efficiency and implementation simplicity.
- **Reward Design.** We propose a Bayesian Information Criterion (BIC)-based reward function that computes the model evidence to evaluate the trade-off between the expression complexity and data fit. This enables the learning process to explicitly optimize the trade-off between interpretability and accuracy, avoiding overly complex expressions that tend to overfit — particularly in the presence of noise. BIC is grounded in Bayesian model selection theory (Wasserman, 2000) and is closely related to the principle of minimum description length (MDL) (Rissanen, 1978), making it a principled and robust criterion. Moreover, BIC introduces no additional hyperparameters, allowing for automatic trade-off adjustment to maximize model evidence, and eliminating the need for manual tuning.
- **Policy Gradient.** We propose a novel risk-seeking policy gradient method, integrated with Group Relative Policy Optimization (GRPO) (Shao et al., 2024). Unlike DSR, which uses reward differences as gradient weights, our approach employs a ranking-based linear weighting scheme to perform step-wise reward mapping. This design not only preserves distinctions among the top-ranked candidates but also avoids any tail barriers or partial tail barriers in the gradient updates. As a result, our method can effectively utilize top-performing samples for model updates, minimizing inefficient or overly exploratory behavior. Furthermore, integration with GRPO enables repeated and reliable optimization steps for each batch of sampled expressions within a trust region, thereby enhancing training effectiveness while reducing sample complexity.
- **Experiments.** We evaluated CADSR on the standard SR benchmark and ablation studies. In addition to DSR, we compared with seventeen other popular and/or state-of-the-art SR methods and several commonly used machine learning approaches. The performance of CADSR in both symbolic discovery and prediction accuracy is consistently among the best. In particular, the symbolic discovery rate of CADSR is the highest when data includes significant noises. In all the cases, CADSR generates the most interpretable expressions, while maintaining a high level of accuracy. CADSR outperforms the most comparable model, DSR, in all categories showing that it is a direct improvement. Extensive ablation studies further demonstrate the effectiveness of each component of our method.

2 Background

Given a set of input and output examples collected from the target system, denoted as $\mathcal{D} = \{(\mathbf{x}_i, y_i)\}_{i=1}^N$, symbolic regression aims to identify a concise expression that characterizes the input-output relationship, such as $y = \sin(2\pi x_1) + \cos(2\pi x_2)$. Deep symbolic regression (DSR) (Petersen et al., 2019) discovers equations via an RNN-based reinforcement learning approach (Sutton and Barto, 2018), which can be broken down into four parts: environment, actor, reward, and policy.

The environment is designed to be the creation of an expression tree that represents a specific equation. Expression trees are directed trees where each node holds a token from the available list of operations and variables, *e.g.*, $\{+, -, \times, /, \sin, \cos, x_1, 1\}$. Expression trees are built by selecting nodes in a preorder traversal of the trees. These trees are many-to-one mappings to the mathematical expressions, which can increase the search space but prevent generating invalid expressions.

The actor is an RNN that predicts a categorical distribution of the available tokens for each node in the expression tree based on the hidden state of the RNN and the sibling and parent of the current node. Each token is randomly sampled from the categorical distribution. Additional rules are applied to the sampling process to prevent the selection of redundant operations or variables.

The reward function and policy drive the actor to explore and exploit the complex environment. In DSR, the reward function is a direct measurement of the data fitness of the generated expression,

$$R(\tau) = \frac{1}{1 + \text{NRMSE}}, \quad (1)$$

where τ denotes the expression, NRMSE represents the normalized root-mean-square error, and is defined as $\text{NRMSE} = \frac{1}{\sigma_y} \sqrt{\frac{1}{n} \sum_{i=1}^n (y_i - \tau(\mathbf{x}_i))^2}$ where σ_y is the standard deviation of the training output in the dataset. DSR applies a risk-seeking policy to update the actor model according to its best predictions. Specifically, at each step, DSR samples a batch of expressions, ranks their rewards, and selects the top $\alpha\%$ expressions to compute a policy gradient,

$$\nabla_{\theta} J_{\text{risk}}(\theta; \alpha) = \frac{1}{\alpha B / 100} \sum_{i=1}^B [R(\tau^{(i)}) - R_{\alpha}] \cdot \mathbf{1}_{R(\tau^{(i)}) \geq R_{\alpha}} \nabla_{\theta} \log(p(\tau^{(i)}|\theta)), \quad (2)$$

where B is the batch size, $\mathbf{1}_{(\cdot)}$ is an indicator function, $\tau^{(i)}$ is the i -th expression in the batch, θ denotes the RNN parameters, $\log(p(\tau^{(i)}|\theta))$ is the probability of $\tau^{(i)}$ being sampled by the current RNN, R_{α} is the $1 - \alpha/100$ quantile of the rewards in the batch. Accordingly, all the equations below top $\alpha\%$ will not influence the update of the actor. This policy enables the actor to generate lower-performing equations without negatively impacting its overall performance, as we only care about the top performed expressions. This allows for more unrestrained exploration and targeted exploitation of the top performers.

3 Method

We now present CADSR, our new deep symbolic regression approach.

3.1 Decoder-Only Expression Generator

We first design a decoder-only transformer architecture for expression generation. Unlike RNNs, which rely on a single hidden state to summarize information across all previous nodes — making them susceptible to vanishing gradients and poor at capturing long-range dependencies (Hochreiter, 1998) — transformers compute dependencies explicitly between all nodes through the attention mechanism. This allows them to overcome the vanishing gradient problem and effectively capture various short- and long-range dependencies.

Dual-Indexed Position Encoding. We use one-hot encoding to represent each token — such as operations, variables, and constants — and adopt an autoregressive approach to generate each node in the expression tree. Instead of assigning a single pre-order index to represent each node, we introduce a dual-indexed position encoding (DPE) to more effectively capture the tree’s structural information. Specifically, given a particular node, we consider both its depth, d , and horizontal location, h , in the tree. To align the horizontal locations of the nodes across different layers, we propose the following design. Denote the horizontal location of the parent node by h_p , if the node is the left child, we assign its horizontal position as $h = h_p - h_p/2^d$, otherwise we assign $h = h_p + h_p/2^d$. In this way, the parent node will be in between its two children horizontally, which naturally reflects the tree structure. The horizontal position for the root node is set to $1/2$. See

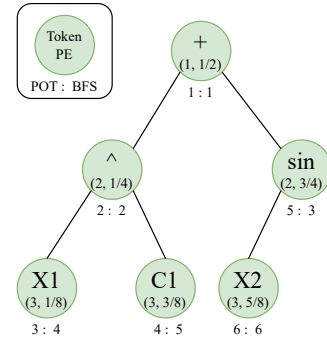


Figure 1: Expression tree for $y = x_1^2 + \sin(x_2)$. POT and BFS denote the node order for preorder traversal and breadth-first-search, respectively.

Fig. 1 for an illustration. We develop a recursive algorithm to efficiently calculate the horizontal positions of all the nodes, as listed in Appendix Algorithm 2. Given d and h , we construct a 2D-dimensional encoding,

$$\text{DPE}(d, h)_{2i} = \sin\left(\frac{d}{10000^{(4i/D)}}\right), \quad \text{DPE}(d, h)_{2i+1} = \cos\left(\frac{d}{10000^{(4i/D)}}\right), \quad (3)$$

$$\text{DPE}(d, h)_{D+2j} = \sin\left(\frac{h}{10^{(4j/D)}}\right), \quad \text{DPE}(d, h)_{D+2j+1} = \cos\left(\frac{h}{10^{(4j/D)}}\right), \quad (4)$$

where $0 \leq i, j \leq \lfloor D/2 \rfloor$. The embedding of each tree node is the positional encoding plus the one-hot encoding of the token.

Robust Attention in Frequency Space. To capture a diverse range of complex, short- and long-range dependencies among tree nodes, we construct multiple self-attention layers. Inspired by the recent DCT-Former model (Scribano et al., 2023) developed for large language models, we propose performing attention in the frequency domain to improve both learning robustness and efficiency. Let the embeddings of the current tree nodes be denoted as $\mathbf{H} = [\mathbf{h}_0, \dots, \mathbf{h}_{N-1}]^\top$, where each $\mathbf{h}_n \in \mathbb{R}^r$ ($0 \leq n \leq N-1$). We treat these embeddings as samples of a function with r -dimensional outputs at N discrete input locations. We then apply a Discrete Cosine-Transform (DCT) to extract their frequency-domain representations $\hat{\mathbf{H}} = [\hat{\mathbf{h}}_0, \dots, \hat{\mathbf{h}}_{N-1}]^\top$, where

$$\hat{\mathbf{H}} = \mathbf{C}\mathbf{H}, \quad C_{k,n} = \alpha_k \cos\left[\frac{\pi}{N} \left(n + \frac{1}{2}\right) k\right]. \quad (5)$$

Here, $0 \leq k, n \leq N-1$, and the normalization constant α_k is defined as $\alpha_k = \sqrt{1/N}$ for $k = 0$, and $\alpha_k = \sqrt{2/N}$ otherwise. The DCT decomposes the function into a weighted sum of cosine basis functions oscillating at different frequencies $k = 0, \dots, N-1$. Each $\hat{\mathbf{h}}_k \in \mathbb{R}^r$ represents the coefficient of the cosine basis at frequency k . One advantage of using the DCT is that the resulting frequency-domain representation remains entirely in the real-valued domain. In contrast, applying a Fourier transform would yield complex-valued representations, requiring special handling to avoid numerical issues. To improve robustness and efficiency during training, we apply a low-pass filter by removing the high-frequency components, which are often associated with noise, outliers in the data, or excessive perturbations to the model parameters. This filtering helps to denoise the representations and stabilize learning. Specifically, we retain only the first M frequency components, denoted as $\hat{\mathbf{H}}_{1:M} = [\hat{\mathbf{h}}_0, \dots, \hat{\mathbf{h}}_{M-1}]^\top$, where M is a tunable hyperparameter. We perform attention on $\hat{\mathbf{H}}_{1:M}$:

$$\hat{\mathbf{A}} = \text{Attention}(\hat{\mathbf{H}}_{1:M}; \mathbf{Q}, \mathbf{K}, \mathbf{V}) = \text{softmax}\left(\frac{(\hat{\mathbf{H}}_{1:M} \cdot \mathbf{Q})(\hat{\mathbf{H}}_{1:M} \cdot \mathbf{K})^\top}{\sqrt{r}}\right)(\hat{\mathbf{H}}_{1:M} \cdot \mathbf{V}). \quad (6)$$

We stack several such self-attention layers in the frequency domain to fully capture the rich, complex dependencies among the frequency components. Then we transform the representation back to the original domain using the inverse DCT:

$$\mathbf{H} \leftarrow \mathbf{C}^\top[\hat{\mathbf{A}}; \mathbf{0}], \quad (7)$$

where the zero-padding restores the original dimensionality by appending $N - M$ frequency components. To predict the token distribution for the next node, we apply a linear layer followed by a softmax function. The overall architecture of our model is illustrated in Appendix Fig. 6.

Expression Sampling. Starting from the root node, we generate the expression tree in a layer-wise, breadth-first-search (BFS) order, auto-regressively expanding the nodes layer by layer. This generation scheme aligns naturally with our dual-indexed positional encoding, enabling effective integration of the spatial relationships between the previously generated nodes and the current target node for token sampling. Moreover, since the tree grows in a fixed layer-by-layer fashion, the ordering of previously generated nodes remains unchanged throughout the process. As a result, we only need to perform vectorization once prior to sampling, making the approach both computationally efficient and straightforward to implement.

Given the predicted token distribution, we first mask out invalid tokens and then sample from the remaining candidates. Once the sampled tokens form a valid expression, the generation process terminates and returns the resulting expression. The complete sampling procedure is summarized in Algorithm 1 in the Appendix.

3.2 BIC Reward Function

Interpretability is a central motivation for symbolic regression. However, when using only data fit as the reward signal — such as in DSR — the model tends to produce overly complex expressions that overfit the data, especially in the presence of noise, which is common in real-world applications. This overfitting undermines the interpretability of the learned expressions. To address this issue, we adopt the Bayesian Information Criterion (BIC) (Schwarz, 1978) to define a new reward function. BIC is theoretically grounded in Bayesian model selection (Wasserman, 2000) and closely related to the Minimum Description Length (MDL) principle (Rissanen, 1978), effectively serving as its approximation.

As a principled and robust criterion, BIC computes the model evidence by integrating out the model parameters, which in essence evaluates the trade-off between the model complexity and data fit in terms of generalizability. In our design, we define the model complexity k as the sum of the number of nodes in the expression tree and the number of constant tokens. This inclusion serves two purposes: (1) Since the values of constant tokens are unknown a priori and must be estimated from data, they effectively act as model parameters, introducing additional degrees of freedom; (2) penalizing the number of constant tokens discourages their excessive use, which would otherwise increase the computational cost of optimizing their values. The BIC reward is defined as:

$$\text{BIC}(\tau) = k \log(S) - 2 \log(p(\tau)), \quad (8)$$

where $\log(p(\tau)) = \sum_{i=1}^S \log \mathcal{N}(y_i | \tau(\mathbf{x}_i), \sigma^2)$ is the Gaussian log-likelihood, σ^2 is the variance of the training outputs, and S is the number of training samples. To accommodate more complex data distributions, $p(\tau)$ can be replaced with a Student- t likelihood or a mixture of Gaussians. Notably, the BIC reward introduces no additional tuning hyperparameters. This allows for automatic balancing between model complexity and data fit, enabling the actor to directly optimize for the expression’s generalizability without manual intervention.

3.3 Robust Risk-Seeking Policy

While our BIC reward (8) accounts for expression complexity, its value is unbounded and can grow arbitrarily large. As a result, directly applying it in a risk-seeking policy framework, as done in DSR, can introduce unpredictable high variance and lead to highly unstable learning. Even after normalization, a few outlier expressions can dominate the reward distribution, causing the majority of well-performing samples to contribute little or nothing to the policy update.

To mitigate this issue, a commonly used strategy, which is also adopted in DSR, is to introduce a continuous mapping that maps the reward value to a bounded domain. For example, DSR uses the mapping $f(z) = \frac{1}{1+z}$ where $z \in [0, \infty]$, which maps the unbounded NRMSE (in $[0, \infty]$) to the range $(0, 1]$; see (1). Another choice can be the sigmoid function, $s(z) = \frac{1}{1+e^{-z}}$ that maps from $(-\infty, \infty)$ to $(0, 1)$. In this way, we can control the variance and improve learning stability. However, this strategy introduces another challenge. That is, the reinforcement learning can encounter a *tail barrier*, defined as follows.

Definition 3.1 (Tail barrier). Let $\alpha \in [0, 1)$. A risk seeking policy meets a α -tail barrier if the top $\alpha\%$ rewards of the sampled actions (e.g., expression trees) are all equal to R_α .

Lemma 3.2. *Given any continuous mapping f that can map unbounded reward function values to a bounded domain (e.g., $(-\infty, \infty) \rightarrow [0, 1]$), suppose the reward function is continuous, there always exists a set of distinct rewards values that numerically create a tail barrier in the risk-seeking policy.*

The proof is given in Appendix Section D.1. In practice, since we often use continuous reward functions (e.g., NRMSE or Gaussian likelihood) and reward mappings, there is a risk of encountering the tail barrier. From (2), we can see that the tail barrier can incur *zero* policy gradient, since all the top $\alpha\%$ rewards are identical to R_α , leading to a zero weight for every gradient. As a consequence, the actor model would not have any effective updates according to the feedback from the selected expressions (top performers). In DSR, the RNN model will be updated only from an entropy bonus term (Petersen et al., 2019), and henceforth the learning starts to explore wildly.

To address this challenge, we introduce a ranking-based linear weighting scheme to construct a step-wise reward mapping,

$$f(z) = \lambda \cdot \text{ReLU} \left(1 - \frac{|\{\tau^{(i)} : R(\tau^{(i)}) > R(z), 1 \leq i \leq B\}|}{\alpha B / 100} \right) \quad (9)$$

where z denotes an arbitrary expression sampled by the actor, $|\cdot|$ represents the size of the set, and $\lambda > 0$ is a scaling constant. This formulation ensures that expressions ranked within the top $\alpha\%$ receive positive mapped rewards, with higher-ranked expressions assigned larger values of $f(z)$, while all other expressions receive a reward of zero. Consequently, only top-performing expressions contribute to the gradient update, and lower-ranked ones are effectively ignored. Our risk-seeking policy gradient is therefore given by

$$\nabla J_{\text{risk}}(\theta; \alpha) \approx \frac{1}{\alpha B / 100} \sum_{i=1}^B f(\tau^{(i)}) \nabla_{\theta} \log p(\tau^{(i)} | \theta). \quad (10)$$

Lemma 3.3. *By using the step function (9) for reward mapping, the policy gradient with our BIC reward, as shown in (10), is unbiased and will not encounter any tail barrier.*

The proof is given in Appendix Section D.2.

Group Relative Policy Optimization. Inspired by the recent success in large language model reasoning, we adapt our policy update into the Group Relative Policy Optimization (GRPO) framework (Shao et al., 2024) to further enhance the learning stability and efficiency. Specifically, among the top $\alpha\%$ candidates, we only use the tokens from those expressions within a trust-region determined by the relative variation in trajectory probability as compared to the earlier model version:

$$\nabla \hat{J}(\theta; \alpha) = \frac{1}{\alpha B / 100} \sum_{i=1}^B f(\tau^{(i)}) \sum_{j=1}^{|\tau^{(i)}|} \nabla_{\theta} \min \left[\frac{p(\tau_j^{(i)} | \tau_{< j}^{(i)}, \theta)}{p(\tau_j^{(i)} | \tau_{< j}^{(i)}, \theta_{\text{old}})}, \text{clip} \left(\frac{p(\tau_j^{(i)} | \tau_{< j}^{(i)}, \theta)}{p(\tau_j^{(i)} | \tau_{< j}^{(i)}, \theta_{\text{old}})}, 1 - \epsilon, 1 + \epsilon \right) \right],$$

where θ_{old} denotes the model parameters at the beginning of the current epoch, $|\tau^{(i)}|$ is the number of tokens in the expression, and $\epsilon \in (0, 1)$ controls the size of the trust-region. This can prevent violent model updates caused by outlier samples. To further improve the learning stability, we introduce a penalty term that penalize model changes that are too aggressive. Our final policy update is given by

$$\nabla J_{\text{GRPO}}(\theta; \alpha) = \nabla \hat{J}(\theta; \alpha) - \frac{100}{\alpha B} \sum_{i=1}^B \sum_{j=1}^{|\tau^{(i)}|} \beta \cdot \nabla \text{KL}[p(\tau_j^{(i)} | \tau_{< j}^{(i)}, \theta) \| p(\tau_j^{(i)} | \tau_{< j}^{(i)}, \theta_{\text{ref}})], \quad (11)$$

where $\text{KL}(\cdot \| \cdot)$ is the Kullback-Leibler divergence, θ_{ref} denotes the parameters of the reference model, which is chosen from a previous epoch, and $\beta > 0$ controls the penalty strength. We use an experience replay buffer (Mnih et al., 2013) to merge the historically best performing $\alpha B / 100$ expressions for each epoch. Our approach is summarized in Appendix Algorithm 4.

4 Related Work

The DSR framework (Petersen et al., 2019) uses reinforcement learning to train an RNN-based expression generator from a given dataset. Recent extensions by Tenachi et al. (2023); Jiang et al. (2024) have incorporated domain knowledge into DSR by enforcing physics-unit constraints or generating rules within a vertical discovery space for vector symbolic regression.

An alternative line of work aims to train foundation models that can map any numerical data directly to symbolic expressions (Biggio et al., 2021; Kamienny et al., 2022; Valipour et al., 2021; Vastl et al., 2022). These approaches typically rely on an encoder-decoder transformer architecture, where the encoder layers extract information from the numerical data, and the decoder layers integrate this information to generate expressions. While promising, such foundation models are expensive to train and highly sensitive to data preparation, which often involves fabricating large-scale synthetic datasets. More importantly, due to the absence of a data-specific search mechanism, these methods may struggle with generalization — particularly when applied to out-of-distribution data (Kamienny et al., 2023). To address this, recent research has explored coupling pretrained foundation models with data-specific search or planning mechanisms to improve expression discovery. Notable examples include TPSR (Shojaee et al., 2023), GPSR (Holt et al., 2023), and GPSR-MCTS (Kamienny et al.,

2023). TPSR integrates a pretrained model within a Monte Carlo Tree Search (MCTS) (Browne et al., 2012) framework, using the model to guide token selection and search tree expansion via an upper confidence bound (UCB) heuristic. The MCTS reward function includes a complexity penalty, controlled by a tunable hyperparameter. GPSR leverages a pretrained encoder-decoder model and employs genetic programming (GP) at inference time, seeding the population with decoder-generated expressions. The top-performing expressions are used to fine-tune the decoder, iterating the GP-finetuning loop until performance plateaus. GPSR-MCTS introduces a mutation policy network — essentially a token generator — enhanced with critic layers to parameterize the MCTS process. The policy network is pretrained on large external datasets and then fine-tuned, along with the critic layers, on the target dataset to discover high-quality expressions.

Other notable efforts include uDSR (Landajuela et al., 2022), an ensemble framework combining multiple symbolic regression methods such as GP and DSR, and model-free approaches (Sun et al., 2023; Xu et al., 2024) that rely solely on MCTS or hybrid strategies combining MCTS and GP for symbolic expression search.

5 Numerical Experiments

For evaluation, we examined CADSR on the comprehensive and well-known SRBench dataset (La Cava et al., 2021), and then conducted an ablation study to assess the effectiveness of each individual component.

5.1 Overall Performance

In SRBench, we first tested on the 133 problems with known solutions. We ran eight trials for each problem at the four *noise* levels: 0%, 0.1%, 1%, and 10%. We ran CADSR in a large computer cluster, for which we set a time limit of 4 hours for each trial. We deployed the trials on NVIDIA A40 GPUs. The maximum number of epochs is set to 600 without early termination. In each epoch, we sampled a batch of 1000 expressions to compute the policy gradient. We used ADAM optimization with initial learning rate was as $1\text{E-}4$. The full list of hyperparameters of our method is provided in Appendix Table 1. We compared with 17 popular and/or state-of-the-art SR methods in terms of Symbolic Solution Rate (%), Accuracy Rate, and Simplified Complexity, which are standard metrics for SR evaluation. These SR baselines include DSR (Petersen et al., 2019), Bingo (Randall et al., 2022), GP-GOMEA (Virgolin et al., 2021), ITEA (de Franca and Aldeia, 2020), TPSR (Shao et al., 2024), BSR (Jin et al., 2020), AIFeynman (Udrescu and Tegmark, 2020), AFP_FE (Schmidt and Lipson, 2009), among others. The majority of these are genetic programming methods with a few notable exceptions: DSR is deep reinforcement learning, TPSR leverages a pretrained foundation model (Kamienny et al., 2022) to conduct Monte-Carlo tree search over expressions, BSR is an MCMC method with a prior placed on the tree structure, and AIFeynman is a divide-and-conquer method that breaks the problem apart by hyper-planes and fits with polynomials. The results of the competing methods are retrieved from the public SRBench report (La Cava et al., 2021) and from published resources. For TPSR, we used the recommended setting of $\lambda = 0.1$, as suggested by the authors, which provides the best trade-off between expression accuracy and complexity. The DSR results reported in the SRBench report correspond to the variant with No Constant Tokens (DSR-NCT), which may not fully capture the method’s performance. To address this, we additionally evaluated an enhanced version of DSR by introducing constant tokens into the token library and optimizing them before each policy update, referred to as DSR-OCT (DSR with Optimized Constant Tokens). The results of all methods are presented in Fig. 2.

Overall, CADSR shows strong performance in symbolic discovery as measured by Symbolic Solution Rate. In particular, when data includes significant noise (10%), CADSR achieves the best solution rate, showing that our method is more *robust* to noise than all the competing methods. Meanwhile, the simplified complexity of our discovered expressions is among the lowest. This together shows that our method, with the BIC reward design, not only can find simpler and hence more interpretable expressions, but also is more resistant to data noise. The Accuracy Rate shows the ratio for which the method is able to discover an equation with $R^2 > 0.999$. CADSR has a competitive accuracy rate with AFP_FE, and Bingo, while outperforming DSR with and without constant optimization. The slightly better methods, such as TPSR and GP-GOMEA, however, generate lengthier and more complex expressions, which lack interpretability and are much far away from the ground truth expression. It is worth noting that CADSR outperforms DSR in both Symbolic Solution Rate (%)

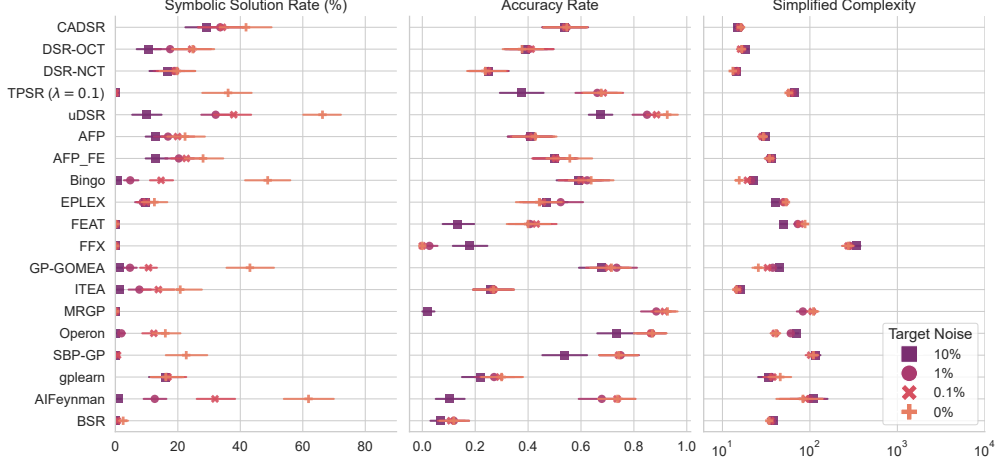


Figure 2: Symbolic regression performance on 133 SRBench problems with known solutions. Error bars denote a 95% confidence region. The numerical values are reported in Appendix Table 5.

and Accuracy Rate, showing an improvement on both expression discovery and prediction accuracy. When data is noise-free, AIFeynman, uDSR, and Bingo shows better Symbolic Solution Rate than CADSR. This might be because: AIFeynman tends to use polynomials to construct the expressions, which match most of the ground-truth; Bingo as a genetic programming approach, uses evolution operators to sample new expressions, which might explore more broadly; uDSR is an ensemble approach using AIFeynman, genetic programming, and DSR and thus can achieve higher symbolic accuracy. However, in the presence of noise, the performance of these methods deteriorates largely and immediately falls behind CADSR, demonstrating CADSR’s superior robustness to noisy data

Next, we tested with the 120 black-box problems in SRBench. Since the true solutions for these problems are *unknown*, we examined the Pareto front of all the methods in Model Size vs. R^2 Test Rank. As shown in Fig. 3, CADSR lies on the Pareto frontier, meaning CADSR is among the best in terms of the trade-off between the model size (expression complexity) and R^2 score (prediction accuracy). On the contrary, methods like Operon and TPSR, typically generates way more complex expressions yet with smaller prediction error. It shows that our method can push the best trade-off toward more interpretability due to BIC penalizing complexity, which can be important in practice.

Runtime. In Appendix Figure 8, we provide a runtime comparison across all the methods. CADSR achieves an average runtime of approximately 4 hours over all problems, which is faster than DCT-OCT and slower than DCT-NCT. Note that DCT-NCT does not involve any constant optimization. On average, Bingo requires around 6 hours, while AIFeynman takes approximately 8 hours. Overall, these results confirm the training efficiency of CADSR.

5.2 Ablation Study

To evaluate the effectiveness of each component of CADSR, we ran ablations on the Feynman dataset from SRBench, which is composed of 119 problems. The numerical values of the metrics are given in Appendix C.

BIC Reward Function: To validate our BIC-based reward function, we first compared it against the standard NRMSE-based reward (see (1)) across varying noise levels. As shown in Figure 4, while the BIC reward performs slightly worse under zero noise, it substantially outper-

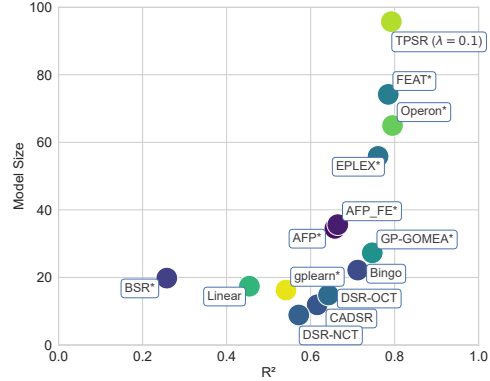


Figure 3: Pareto front of each method in 120 black-box problems of SRBench; the true solutions are unknown. Numerical metrics are reported in Appendix Table 6.

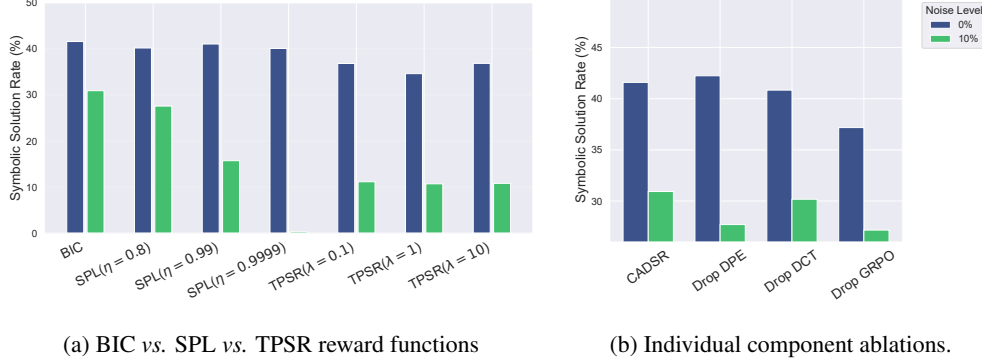


Figure 5: Symbolic Solution Rate of CADSR with (a) alternative reward function and (b) individual component removes on Feynman dataset.

forms the NRMSE-based reward at all other noise levels. Notably, at a 10% noise level, the BIC reward improves upon the NRMSE-based reward by 111% in Symbolic Solution Rate. In addition, we evaluated our BIC reward against two recently proposed alternatives: the SPL (Sun et al., 2023) and TPSR (Shojaee et al., 2023) reward functions, which both incorporate an explicit trade-off hyperparameter to balance expression complexity and data fit — denoted by η in SPL and λ in TPSR. Definitions of these rewards are provided in (12) and (13) in the Appendix. We performed the comparison at noise levels of 0% and 10%, testing a range of values for the trade-off hyperparameters. As shown in Figure 5a, our BIC reward — which requires no manually tuned trade-off parameter — consistently outperforms both alternatives across all settings. Specifically, the SPL reward achieves its highest Symbolic Solution Rate at $\eta = 0.99$ (for 0% noise) and $\eta = 0.8$ (for 10% noise), yet still falls short by 0.5% and 3%, respectively, compared to our BIC reward. The TPSR reward reaches its peak at $\lambda = 0.1$ for both noise levels, trailing our method by 5% and 20%. These results highlight the strength of our BIC-based approach, particularly in noisy settings, and confirm its effectiveness in balancing complexity and data fidelity without requiring parameter tuning

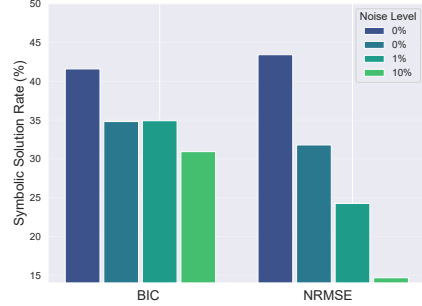


Figure 4: CADSR performance the standard NRMSE reward function.

Other Components: Next, we conducted an ablation study by individually removing other components from CADSR to evaluate their contributions to overall performance. Specifically, we replaced the DCT attention layer (see (5) and (6)) with a standard attention mechanism, substituted the dual-indexed position encoding (DPE) with a 1D positional encoding, and replaced GRPO with a standard risk-seeking policy gradient. The comparative results are presented in Figure 5b. As shown, removing each component generally led to a performance drop. The only exception was replacing DPE with 1D positional encoding, which resulted in a slight improvement of 0.5% in the noise-free setting; however, at the 10% noise level, performance declined by 3%. The DCT attention module not only improved the Symbolic Solution Rate compared to standard attention, but also reduced expression sampling time (see C.2 for runtime details). GRPO had a substantial impact: its removal decreased the symbolic discovery rate by 4.5%, and also slowed convergence — with the final expression discovered at an average of epoch 257, compared to epoch 168 with GRPO. Detailed convergence plots are provided in Appendix C.3.

6 Conclusion

We have presented CADSR, a new symbolic regression approach based on reinforcement learning. On standard SR benchmark problems, CADSR shows promising performance. The ablation study confirms the effectiveness of each component of our method. Nonetheless, our current work has two limitations. First, the implementation is inefficient, especially for expression optimization, as each expression is optimized in sequence rather than parallel, causing a slow training process. Second, we lack an early stopping mechanism to reduce the training cost further and prevent useless exploration. In the future, we plan to address these limitations and examine our method in practical applications.

References

- Biggio, L., Bendinelli, T., Neitz, A., Lucchi, A., and Parascandolo, G. (2021). Neural symbolic regression that scales. In International Conference on Machine Learning (ICML), pages 936–945. Pmlr.
- Bomarito, G., Leser, P., Strauss, N., Garbrecht, K., and Hochhalter, J. (2023). Automated learning of interpretable models with quantified uncertainty. Computer Methods in Applied Mechanics and Engineering, 403:115732.
- Browne, C. B., Powley, E., Whitehouse, D., Lucas, S. M., Cowling, P. I., Rohlfshagen, P., Tavener, S., Perez, D., Samothrakis, S., and Colton, S. (2012). A survey of monte carlo tree search methods. IEEE Transactions on Computational Intelligence and AI in games, 4(1):1–43.
- Burlacu, B., Kronberger, G., and Kommenda, M. (2020). Operon C++: an efficient genetic programming framework for symbolic regression. In Proceedings of the 2020 Genetic and Evolutionary Computation Conference Companion, GECCO '20, pages 1562–1570, New York, NY, USA. Association for Computing Machinery.
- de Franca, F. O. and Aldeia, G. S. I. (2020). Interaction-Transformation Evolutionary Algorithm for Symbolic Regression. Evolutionary Computation, pages 1–25.
- Hochreiter, S. (1998). The Vanishing Gradient Problem During Learning Recurrent Neural Nets and Problem Solutions. International Journal of Uncertainty, Fuzziness and Knowledge-Based Systems, 06(02):107–116. Publisher: World Scientific Publishing Co.
- Holt, S., Qian, Z., and van der Schaar, M. (2023). Deep generative symbolic regression. In The Eleventh International Conference on Learning Representations.
- Jiang, N., Nasim, M., and Xue, Y. (2024). Vertical symbolic regression via deep policy gradient. In Proceedings of the Thirty-Third International Joint Conference on Artificial Intelligence (IJCAI), pages 5891–5899.
- Jin, Y., Fu, W., Kang, J., Guo, J., and Guo, J. (2020). Bayesian symbolic regression.
- Jobin, A., Ienca, M., and Vayena, E. (2019). The global landscape of AI ethics guidelines. Nature Machine Intelligence, 1(9):389–399. Publisher: Nature Publishing Group.
- Kamienny, P.-A., d’Ascoli, S., Lample, G., and Charton, F. (2022). End-to-end Symbolic Regression with Transformers.
- Kamienny, P.-A., Lample, G., Lamprier, S., and Virgolin, M. (2023). Deep generative symbolic regression with monte-carlo-tree-search. In International Conference on Machine Learning, pages 15655–15668. PMLR.
- Kingma, D. P. and Ba, J. (2017). Adam: A method for stochastic optimization.
- Koza, J. R. (1994). Genetic programming as a means for programming computers by natural selection. Statistics and Computing, 4(2):87–112.
- La Cava, W., Orzechowski, P., Burlacu, B., de Francca, F. O., Virgolin, M., Jin, Y., Kommenda, M., and Moore, J. H. (2021). Contemporary Symbolic Regression Methods and their Relative Performance. arXiv:2107.14351 [cs].
- Landajuela, M., Lee, C., Yang, J., Glatt, R., Santiago, C. P., Aravena, I., Mundhenk, T. N., Mulcahy, G., and Petersen, B. K. (2022). A unified framework for deep symbolic regression. In Oh, A. H., Agarwal, A., Belgrave, D., and Cho, K., editors, Advances in Neural Information Processing Systems.
- Levenberg, K. (1944). A method for the solution of certain non-linear problems in least squares. Quarterly of Applied Mathematics, 2(2):164–168.
- Mnih, V., Kavukcuoglu, K., Silver, D., Graves, A., Antonoglou, I., Wierstra, D., and Riedmiller, M. (2013). Playing atari with deep reinforcement learning.

- Petersen, B. K., Landajuela, M., Mundhenk, T. N., Santiago, C. P., Kim, S. K., and Kim, J. T. (2019). Deep symbolic regression: Recovering mathematical expressions from data via risk-seeking policy gradients.
- Randall, D. L., Townsend, T. S., Hochhalter, J. D., and Bomarito, G. F. (2022). Bingo: a customizable framework for symbolic regression with genetic programming. In Proceedings of the Genetic and Evolutionary Computation Conference Companion, GECCO '22, pages 2282–2288, New York, NY, USA. Association for Computing Machinery.
- Rissanen, J. (1978). Modeling by shortest data description. Automatica, 14(5):465–471.
- Rudin, C. (2019). Stop Explaining Black Box Machine Learning Models for High Stakes Decisions and Use Interpretable Models Instead. arXiv:1811.10154 [cs, stat].
- Schmidt, M. and Lipson, H. (2009). Distilling Free-Form Natural Laws from Experimental Data. Science, 324(5923):81–85. Publisher: American Association for the Advancement of Science.
- Schwarz, G. (1978). Estimating the dimension of a model. The annals of statistics, pages 461–464.
- Scribano, C., Franchini, G., Prato, M., and Bertogna, M. (2023). Dct-former: Efficient self-attention with discrete cosine transform. Journal of Scientific Computing, 94(3).
- Shao, Z., Wang, P., Zhu, Q., Xu, R., Song, J., Bi, X., Zhang, H., Zhang, M., Li, Y. K., Wu, Y., and Guo, D. (2024). Deepseekmath: Pushing the limits of mathematical reasoning in open language models.
- Shojaee, P., Meidani, K., Farimani, A. B., and Reddy, C. K. (2023). Transformer-based Planning for Symbolic Regression.
- Sun, F., Liu, Y., Wang, J.-X., and Sun, H. (2023). Symbolic physics learner: Discovering governing equations via monte carlo tree search. In The Eleventh International Conference on Learning Representations.
- Sutton, R. S. and Barto, A. G. (2018). Reinforcement learning: An introduction. MIT press.
- Tamar, A., Glassner, Y., and Mannor, S. (2014). Policy Gradients Beyond Expectations: Conditional Value-at-Risk.
- Tenachi, W., Ibata, R., and Diakogiannis, F. I. (2023). Deep symbolic regression for physics guided by units constraints: toward the automated discovery of physical laws. The Astrophysical Journal, 959(2):99.
- Udrescu, S.-M. and Tegmark, M. (2020). AI Feynman: a Physics-Inspired Method for Symbolic Regression. arXiv:1905.11481 [hep-th, physics:physics].
- Valipour, M., You, B., Panju, M., and Ghodsi, A. (2021). SymbolicGPT: A Generative Transformer Model for Symbolic Regression. arXiv:2106.14131 [cs].
- Vastl, M., Kulhánek, J., Kubalík, J., Derner, E., and Babuvska, R. (2022). SymFormer: End-to-end symbolic regression using transformer-based architecture. arXiv:2205.15764 [cs].
- Virgolin, M., Alderliesten, T., Witteveen, C., and Bosman, P. A. N. (2021). Improving Model-based Genetic Programming for Symbolic Regression of Small Expressions. Evolutionary Computation, 29(2):211–237. arXiv:1904.02050 [cs].
- Wasserman, L. (2000). Bayesian model selection and model averaging. Journal of mathematical psychology, 44(1):92–107.
- Xu, Y., Liu, Y., and Sun, H. (2024). Reinforcement symbolic regression machine. In The Twelfth International Conference on Learning Representations.

Appendix

A Algorithms

Below, we show the algorithms for expression sampling and positional encoding generation. Note that for expression sampling, we over-sample expressions so that we can return a high number of unique ones. If not enough unique expressions exist, then we begin to allow duplicates to fill out our batch size requirements.

Algorithm 1 Expression Tree Sampling

input Number of expressions to sample B ; oversampling scalar $\gamma > 1$, maximum tree-node number ν

output A set of expressions \mathcal{T}

```
1:  $\mathcal{T} \leftarrow \text{ExpressionTrees}(\gamma B)$  {Creates  $\gamma B$  empty expression trees}
2: while  $i < \nu$  do
3:    $V_{\mathcal{T}} \leftarrow \text{Inputs}(\mathcal{T})$  {Fetching the input embeddings of all the expression trees}
4:    $S \leftarrow p(V_{\mathcal{T}}|\theta)$  {Predicting categorical distributions from the transformer}
5:    $S \leftarrow R(S)$  {Applying rules to each distribution}
6:    $K \leftarrow P(\cdot|S)$  {Sampling from the categorical distribution to obtain tokens}
7:    $\mathcal{T}_i \leftarrow K$  {Adding the new tokens into the expression trees}
8: end while
9:  $\mathcal{T} = \text{Unique}(\mathcal{T}, B)$  {Take the first  $B$  Unique expression trees}
10: return  $\mathcal{T}$ 
```

Algorithm 2 Dual Indexed Position Encoding (DPE) Generation

input An expression tree τ

```
1:  $\tau.\text{root\_node}.\text{depth} = 1$ 
2:  $\tau.\text{root\_node}.\text{horizontal} = 1/2$ 
3:  $\text{PositionEncodingInformation}(\tau.\text{root\_node})$ 
```

Algorithm 3 PositionEncodingInformation

input Current node

```
1: if node has left then
2:    $\text{node}.\text{left}.\text{depth} = \text{node}.\text{depth} + 1$ 
3:    $\text{node}.\text{left}.\text{horizontal} = \text{node}.\text{horizontal} - 1/(2^{\text{node}.\text{left}.\text{depth}})$ 
4:    $\text{PositionEncodingInformation}(\text{node}.\text{left})$ 
5: end if
6: if node has right then
7:    $\text{node}.\text{right}.\text{depth} = \text{node}.\text{depth} + 1$ 
8:    $\text{node}.\text{right}.\text{horizontal} = \text{node}.\text{horizontal} + 1/(2^{\text{node}.\text{right}.\text{depth}})$ 
9:    $\text{PositionEncodingInformation}(\text{node}.\text{right})$ 
10: end if
```

B Model Details

Table 1 and Fig. 6 show the comprehensive hyperparameter settings and the architecture of the transformer used in CADSR. Note that we use the Levenberg–Marquardt algorithm (Levenberg, 1944) to optimize the constant tokens for each discovered equation and used Adam (Kingma and Ba, 2017) to optimize the model.

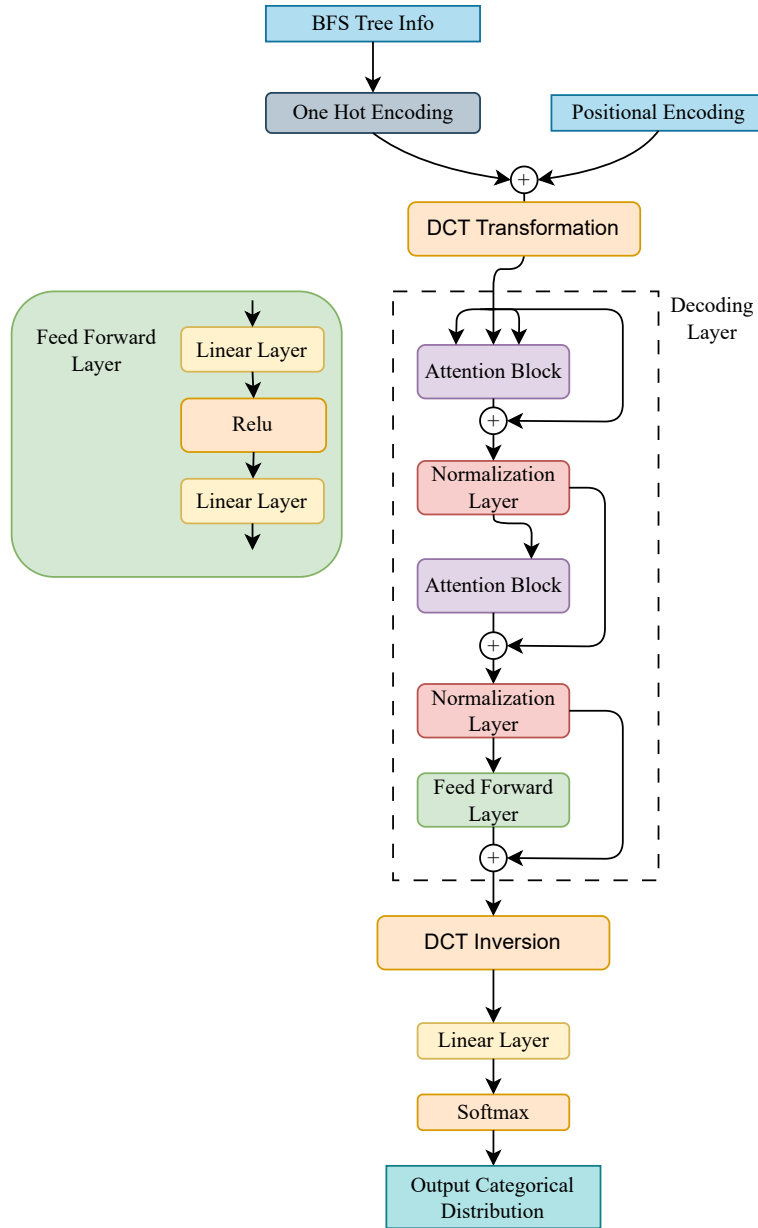


Figure 6: The architecture of the transformer actor in CADSR.

Algorithm 4 Complexity-Aware Deep Symbolic Regression (CADSR)

input Learning rate l ; risk factor α ; batch size B ; coefficients $\lambda > 0$; steps per epoch C ; epochs per reference G ; number of epochs T

output The best equation τ^*

```
1: Initialize transformer with parameters  $\theta$ 
2: while  $i < T$  do
3:   if  $i \bmod(G) = 0$  then
4:      $\theta_{\text{ref}} \leftarrow \theta$     {Set the reference weights to the current weights}
5:   end if
6:    $\theta_{\text{old}} \leftarrow \theta$     {Set the old weights to the current weights}
7:    $\mathcal{T} \leftarrow \{\text{OptimizeConstants}(\tau^{(i)}) : \tau^{(i)} \sim p(\cdot|\theta)\}_{i=1}^B$  {Sample  $B$  expressions from the transformer actor and optimize the values of constant tokens}
8:    $\mathcal{R} \leftarrow \{\text{BIC}(\tau^{(i)})\}_{i=1}^B$  {Calculate the reward for each expression using (8)}
9:    $\mathcal{R}_\alpha \leftarrow (1 - \alpha/100)\text{-quantile of } \mathcal{R}$ 
10:   $\mathcal{T} \leftarrow \{\tau^{(i)} : \mathcal{R}(\tau^{(i)}) \geq \mathcal{R}_\alpha\}$  {Pick top  $\alpha\%$  expressions}
11:   $\mathcal{T} \leftarrow \mathcal{T} \cup \mathcal{T}_{\text{historical}}$  {Merge with the historical top performing expressions}
12:  for  $j = 1$  to  $C$  do
13:     $\theta \leftarrow \theta + l \cdot (\nabla_{\theta} J_{\text{GRPO}} + \lambda_{\mathcal{H}} \cdot \text{Entropy-Bonus})$  {Compute the policy gradient using (11); the entropy bonus term comes from the original DSR.}
14:    if  $\max \mathcal{R} > \mathcal{R}(\tau^*)$  then  $\tau^* \leftarrow \tau^{(\arg\max \mathcal{R} \in \mathcal{T})}$  {Update the best equation}
15:  end for
16:   $\mathcal{T}_{\text{historical}} \leftarrow \text{Top } \alpha\% \text{ of the expressions in } \mathcal{T}$  {Update the experience replay buffer}
17:   $i \leftarrow i + 1$ 
18: end while
19: return  $\tau^*$ 
```

Table 1: Hyperparameter settings of CADSR.

Hyperparameter	CADSR
Variables	$\{1, c \text{ (Constant Token)}, x_i\}$
Unary Functions	$\{\sin, \cos, \log, \sqrt{(\cdot)}, \exp\}$
Binary Functions	$\{+, -, *, /, ^\wedge\}$
Batch Size	1000
Risk Seeking Percent (α)	5%
Learning Rate	1E-4
Max Depth	32
Oversampling	2 (Ideally 3)
Number of Epochs	600
Policy	BIC
λ	0.2
Entropy Coefficient $\lambda_{\mathcal{H}}$	0.005
Encoder Number	0
Decoder Number	1
Number of Heads	1
Feed Forward Layers Size	2048
β	0.01
ϵ	0.2
Embedding Dim	15
DCT Clip Dim	12
C	5
G	5

C Additional Ablation Analysis

C.1 Ablation Reward Functions

SPL and TPSR introduced reward functions with regularization terms and tunable hyperparameters. SPL’s reward function is specified in (12), and TPSR’s reward function is (13). SPL introduced a

Table 2: Hyperparameter settings for DSR

<i>Hyperparameter</i>	<i>DSR</i>
Batch Size	100
Learning Rate	0.0005
Entropy coefficient	0.005
Risk Factor Percent	5%
RNN Type	LSTM
Layer Number	1

Table 3: Performance of CADSR for each Ablation on the Feynman Dataset

Algorithm	Symbolic Solution Rate (%)	
	0.0%	10%
CADSR	41.59	30.93
Drop DPE	42.24	27.69
Drop BIC	43.43	14.65
Drop DCT	40.84	30.17
Drop GPRO	37.18	27.16
SPL ($\eta = 0.8$)	40.19	27.59
SPL ($\eta = 0.99$)	41.06	15.73
SPL ($\eta = 0.9999$)	40.09	0.32
TPSR ($\lambda = 0.1$)	36.83	11.16
TPSR ($\lambda = 1$)	34.62	10.71
TPSR ($\lambda = 10$)	36.85	10.81

scalar term η^n , where n denotes the number of multiplication operators in the expression, and η is a hyperparameter. η controls the strength of the regularizer where $\eta = 1$ means no regularization and $\eta < 1$ strengthens the regularization. The authors of the SPL work found that tuning η significantly impacts the performance, and they suggest a starting value of $\eta = 0.99$. TPSR introduced an additive term $\lambda \exp(\frac{-l(\tau)}{L})$, where L is the max number of tokens, $l(\tau)$ is the length of the expression, and λ is a hyperparameter. λ controls the regularization, and having a large λ will increase the regularization.

$$R(\tau) = \frac{\eta^n}{1 + \sqrt{\frac{1}{N} \sum_{i=1}^N (y_i - \tau(\mathbf{x}_i))^2}} \quad (12)$$

$$R(\tau) = \frac{1}{1 + \text{NMSE}(y, \tau(\mathbf{x}))} + \lambda \exp(\frac{-l(\tau)}{L}) \quad (13)$$

C.2 DCT Attention

The DCT converts the input into the signal space before using the attention mechanism, which maintains the transformer’s time complexity of $\mathcal{O}(n^2d)$, where n is the sequence length and d is the embedding dimension. We reduce the embedding space by clipping the highest frequency components. For SRBench, we clipped the 2 highest frequency signals from a 10-dimensional embedding space. Therefore, we should attain around a 20% decrease in sampling time of the standard transformer. Since the runtime for the whole SRBench is dominated by the optimization of the constant token(s), to exclusively evaluate the sampling efficiency, we tested with the Nguyen-4 problem, which does not include the constant token in the token library. We ran our method with DCT attention layers and with ordinary attention layers, each for 50 trials with 100 epochs per trial on an RTX 3080 GPU. We recorded the time each architecture took to predict tokens. The empirical results, as shown in Table 4, match the theoretical runtime reduction, resulting in a 21% decrease in sample time using the DCT attention layers.

C.3 GRPO

We observed that GRPO can increase performance and convergence rate compared to the standard risk-seeking gradient. Figure 7 includes 20 random problems from Feynman dataset in SRBench. We

Table 4: Sampling Time on Nguyen-4 with 50 trials.

Architecture	Total Sample Time (s)	Sample Time per Expression (ms)
DCT attention	1072.8	3.576
Standard attention	1354.2	4.514

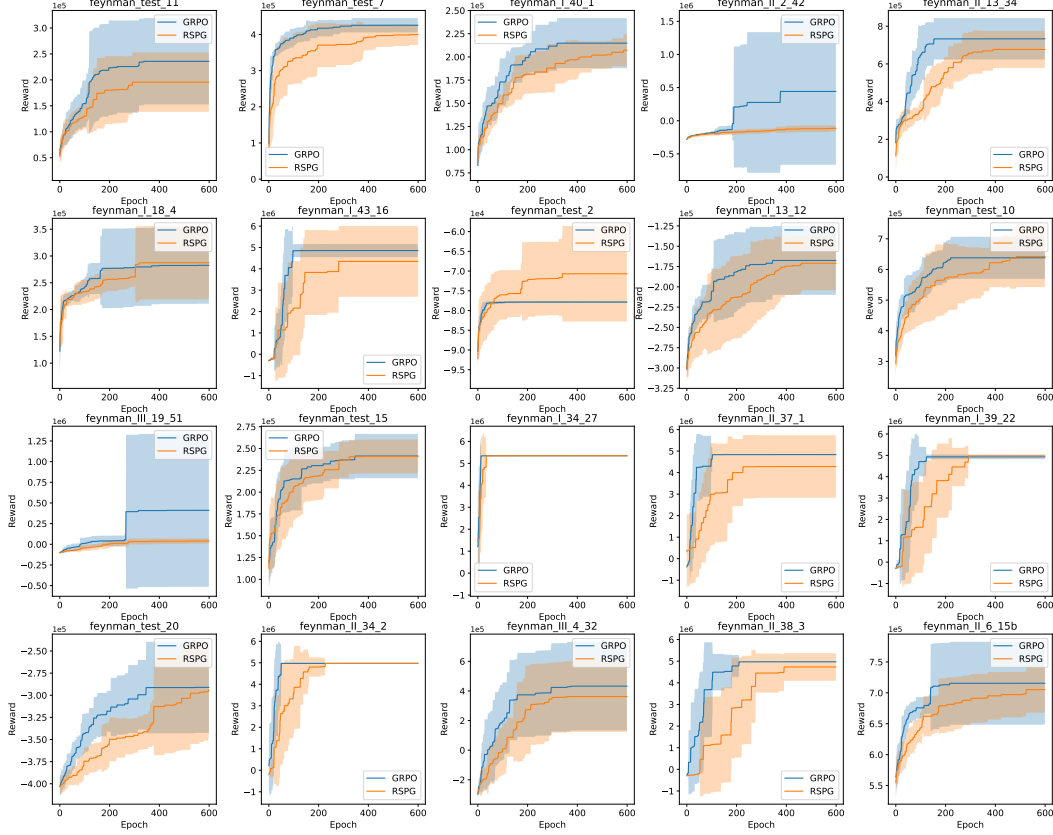


Figure 7: Twenty examples of learning curves (the number of epochs vs. reward) for running CADSR with GRPO and with standard risk seeking policy gradient (RSPG). The problems were randomly selected from the Feynman dataset. Errors are one standard deviation.

can see in all the cases, GRPO enables the model to converge faster than the standard risk-seeking policy gradient. In the vast majority of the case, GRPO leads to a higher reward. On average, GRPO improves the symbolic recovery rate across the entire dataset.

D Theoretical Results

D.1 Proof of Lemma 3.2

Proof. Pick up any reward value z_0 . Due to the continuity of the mapping f , for arbitrary $\epsilon > 0$, there exists $\delta > 0$ such that for all $z \neq z_0$, if $|z - z_0| < \delta$, then $|f(z) - f(z_0)| < \epsilon$. Let us take $\epsilon = \frac{1}{2}s$, where s is the machine precision (e.g., 2^{-32}). Since the reward function is continuous, we can find a set of distinct reward values z_1, \dots, z_M from $B(z_0, \delta(\epsilon)) = \{z \in \text{dom } f, |z - z_0| < \delta(\epsilon)\}$. Let us look at the mapped rewards, $f(z_1), \dots, f(z_M)$. For any $1 \leq i, j \leq M$, we have

$$|f(z_i) - f(z_j)| = |f(z_i) - f(z_0) + f(z_0) - f(z_j)| \leq |f(z_i) - f(z_0)| + |f(z_0) - f(z_j)| < \frac{s}{2} + \frac{s}{2} = s.$$

Therefore, there are no numerical difference among these mapped rewards, and they can create a tail barrier. \square

D.2 Proof of Lemma 3.3

Proof. For any set of BIC reward values, $\mathcal{S} = \{R(\tau^{(1)}), \dots, R(\tau^{(B)})\}$, we denote the mapped reward values by $\hat{\mathcal{S}} = \{\hat{R}_1, \dots, \hat{R}_B\}$, where each $\hat{R}_j = f(R(\tau^{(j)}))$ ($1 \leq j \leq B$). We know that each

$$\hat{R}_j = \lambda \cdot \text{ReLU} \left(1 - \frac{|\{\tau^{(i)} : R(\tau^{(i)}) > R(\tau^{(j)}), 1 \leq i \leq B\}|}{B\alpha/100} \right) \quad (14)$$

where R_α is the $1 - \frac{\alpha}{100}$ quantile of the rewards in \mathcal{S} . Let B_α denotes the number of top $\alpha\%$ expressions. We have $B\alpha/100 = B_\alpha$, and

$$\hat{R}_j = \lambda \cdot \text{ReLU} \left(1 - \frac{|\{\tau^{(i)} : R(\tau^{(i)}) > R(\tau^{(j)}), 1 \leq i \leq B\}|}{B_\alpha} \right).$$

Since for every top $\alpha\%$ expression $\tau^{(j)}$, the numerator $|\{\tau^{(i)} : R(\tau^{(i)}) > R(\tau^{(j)}), 1 \leq i \leq B\}|$ is an integer and is guaranteed to be less than B_α , \hat{R}_j is always positive. Accordingly, every expression in the top $\alpha\%$ will not have their gradient zeroed out (see (10)), and we will never meet a tail or partial tail barrier.

To show the unbiasedness, we need to replace R_α by the $1 - \alpha/100$ quantile of the distribution of the BIC reward R . Denote the mapped reward by \hat{R} . Since \hat{R} is bounded, namely, $\hat{R} \in [0, 1]$, we can follow exactly the same steps in the proof of the original risk-adverse gradient paper (Tamar et al., 2014) to show the unbiasedness of (10). \square

E SRBench

E.1 Symbolic Problems

We provide Table 5 containing the numerical values for all of the algorithms for all of the algorithms we compare within Figure 2. Bolded values are the best for the given column. CADSR has achieved the best performance for 0.1%, 1%, and 10% noise, generating the second most simple models on average for these noise levels. MRGP has the best performance in terms of accuracy but generates overly complex expressions with high accuracy. Note that uDSR is omitted because its exact numerical data is not available. SRBench uses SymPy¹ to evaluate symbolic accuracy. However, SymPy is known for generating false negatives due to incomplete simplifications. For our table, we also counted any expression as being symbolically correct when the R^2 test score is exactly 1.0, as it is improbable that an expression that is not symbolically equivalent will perfectly predict at $\sim 20,000$ testing points.

E.2 Black Box Problems

Table 6 shows the numerical performance metrics and runtimes of each method tested on the black box SRBench dataset. While CADSR does not give the best metric in any category, it does appear on the Pareto front in Figure 3. Notably, SBP-GP, TPSR, and Operon are the best-performing algorithms in terms of R^2 test score on the black box problems and have a higher level of complexity than CADSR. SBP-GP and Operon are GP-based methods. TPSR is a transformer that uses MCTS on a pretrained transformer to predict lengthy and accurate expressions.

F Run Times

Figure 8 shows the recorded runtime of each method in solving the symbolic problems from SRBench. However, this is a rough comparison, since CADSR does not use any early stopping criterion and the hardware resources — though comparable — are not exactly the same across all the methods for this benchmark.

¹<https://www.sympy.org/en/index.html>

Table 5: Symbolic regression performance in SRBench with known solutions.

Algorithm	Symbolic Solution Rate (%)				Accuracy Rate (%)				Simplified Complexity			
	0.0%	0.1%	1%	10%	0.0%	0.1%	1%	10%	0.0%	0.1%	1%	10%
AFP	22.31	19.92	16.85	12.85	43	42	40	41	29.35	28.43	29.01	30.82
AFP_FE	28.08	22.69	20.31	12.85	56	50	50	50	34.58	35.66	34.45	36.77
AlFeynman	61.84	31.89	12.61	0.86	74	74	68	10	83.29	88.66	99.27	110.54
BSR	2.50	0.61	0.08	0.00	12	11	12	7	34.29	35.51	36.80	38.38
Bingo	48.77	14.62	4.77	0.77	64	60	62	59	15.56	19.29	21.32	22.54
CADSR	41.83	34.27	33.57	29.25	55	54	55	54	16.30	15.69	15.89	15.03
DSR-OCT	24.81	24.42	17.53	10.48	38	41	40	39	16.57	16.10	16.96	18.45
DSR-NCT	19.71	19.23	18.92	16.61	24	25	25	25	13.14	14.36	14.61	14.40
EPLEX	12.50	9.92	8.77	9.54	44	45	52	47	53.24	51.74	49.91	40.04
FEAT	0.10	0.00	0.00	0.00	40	43	41	14	88.01	77.32	72.61	50.40
FFX	0.00	0.00	0.00	0.08	0	0	3	18	274.88	273.29	286.03	341.38
GP-GOMEA	43.08	10.62	4.69	1.46	71	70	73	68	25.73	32.75	37.59	45.41
ITEA	20.77	13.77	7.69	1.46	27	27	27	26	14.46	14.96	15.35	16.00
MRGP	0.00	0.00	0.00	0.00	93	92	89	2	109.95	106.50	83.06	0.00
Operon	16.00	12.31	1.92	0.08	87	86	86	73	40.80	40.13	60.40	70.78
SBP-GP	22.69	0.69	0.00	0.00	74	74	75	54	109.94	102.09	112.93	116.30
TPSR	36.09	0.00	0.00	0.00	68	68	66	38	57.11	59.32	63.42	65.83
gplearn	16.15	16.86	16.59	16.00	30	29	27	22	45.80	37.76	36.42	33.84

Table 6: Symbolic regression performance and runtime on black box problems in SRBench.

Algorithm	R ² Test	Model Size	Training Time (s)
AFP	0.657613	34.5	6002.55
AFP_FE	0.664599	35.6	6153.50
AlFeynman	-3.745132	2500	82069.31
AdaBoost	0.704752	10000	65.29
BSR	0.257598	19.8	20426.86
Bingo	0.711951	22.2	53537.42
CADSR	0.615459	11.9	5643.43
DSR-NCT	0.571669	8.89	35096.16
DSR-OCT	0.642417	14.8	4267.68
EPLEX	0.760414	55.8	15673.69
FEAT	0.784662	74.2	6723.91
FFX	-0.667716	1570	243.74
GP-GOMEA	0.746634	27.3	9063.54
ITEA	0.640731	112	12337.48
KernelRidge	0.615147	1820	38.88
LGBM	0.637670	5500	28.53
Linear	0.454174	17.4	0.24
MLP	0.531249	3880	30.47
MRGP	0.417864	12100	190697.78
Operon	0.794831	65.0	2979.43
RandomForest	0.698541	1.54e+06	120.21
SBP-GP	0.798932	639	166745.46
TPSR	0.792001	95.7	504.38
XGB	0.775793	16400	240.58
gplearn	0.541264	16.3	24157.99

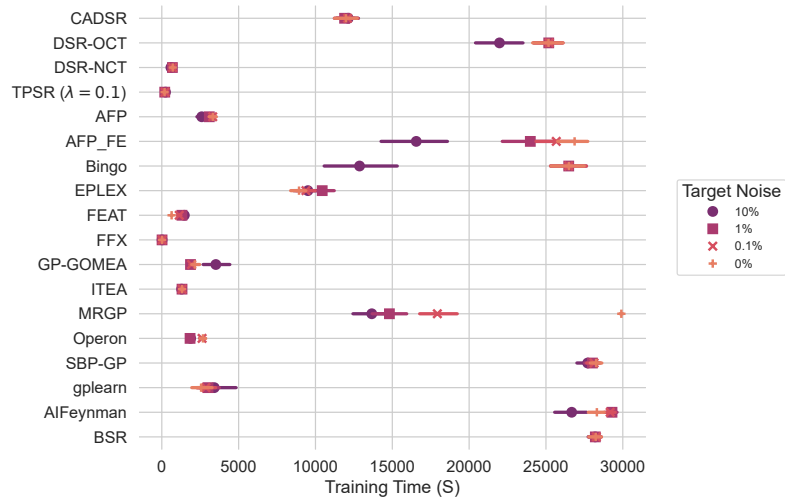


Figure 8: Runtime in solving SRBench problems with solutions known. Error bars denote a 95% confidence interval.